

Bucking Coil Implementation on PMT for Active Cancelling of Magnetic Field

T. Gogami^a, A. Asaturyan^b, J.Bono^c, P.Baturin^c, C. Chen^d, A. Chiba^a, N. Chiga^a, Y. Fujii^a,
O. Hashimoto^{a*}, D. Kawama^{a†}, T. Maruta^{a‡}, V.Maxwell^c, A. Mkrtchyan^b, S. Nagao^a,
S. N. Nakamura^a, J. Reinhold^c, A. Shichijo^a, L. Tang^d, N. Taniya^a, S. A. Wood^e, Z. Ye^d

a) Graduate School of Science, Tohoku University, Sendai, 980-8578, Japan

b) Yerevan Physics Institute, Armenia

c) Department of Physics, Florida International University, Miami, Florida 33199, USA

d) Department of Physics, Hampton University, Virginia 23668, USA

e) Thomas Jefferson National Accelerator Facility, Newport News, Virginia 23606, USA

Abstract

Aerogel and water Čerenkov detectors were employed to tag kaons for a Λ hypernuclear spectroscopic experiment which used the $(e, e'K^+)$ reaction in experimental Hall C at Jefferson Lab (JLab E05-115). Fringe fields from the kaon spectrometer magnet yielded ~ 5 Gauss at the photomultiplier tubes (PMT) for these detectors which could not be easily shielded. As this field results in a lowered kaon detection efficiency, we implemented a bucking coil on each photomultiplier tubes to actively cancel this magnetic field, thus maximizing kaon detection efficiency.

1 Introduction

We performed a Λ hypernuclear spectroscopic measurement, which used the $(e, e'K^+)$ reaction at JLab Hall-C in 2009 (JLab E05-115 [1][2]). The scattered electron (e') and kaon (K^+) were measured in coincidence using the HES (High resolution Electron Spectrometer) and HKS (High resolution Kaon Spectrometer), dedicated electron and kaon spectrometers. The positions and angles of the scattered particles were measured with tracking detectors in the focal planes of each spectrometer and this information was used to reconstruct a missing mass.

However, HKS, the kaon spectrometer, had a very large background of protons and positive pions. An

aerogel Čerenkov detector and a water Čerenkov detector, used to reject π^+ s and protons both on-line and off-line, played an important role in K^+ identification. These Čerenkov detectors were mounted close to the HKS dipole magnet (Figure 1) in order to minimize loss of kaons due to decay. Therefore, fringe field of up to ~ 5 G were observed in the region of the photomultiplier tubes (PMTs) on the Čerenkov detectors. It was expected that the K^+ identification efficiency would be reduced because of the effects of magnetic fields on PMT performance. A previous experiment

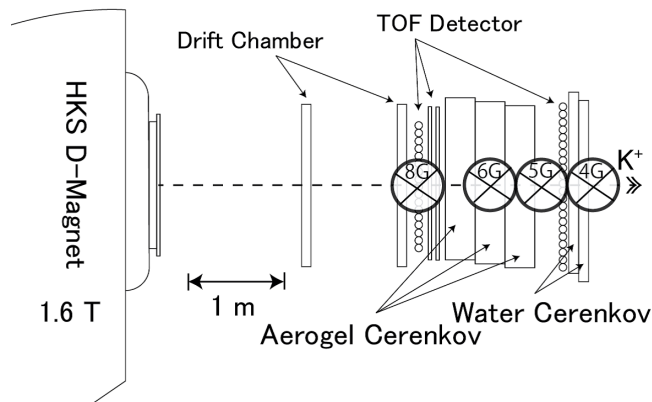


Figure 1: A schematic drawing of the HKS detectors of JLab E05-115. The fringe field of HKS dipole magnet (normal conducting magnet, 1.6 T) which is 4~6 G around the Čerenkov detectors effects on their PMT performance.

(JLab E01-011 [3][4][5][6] in 2005) used iron shields around the PMTs. However, this was not optimal as it is difficult to shield magnetic fields parallel to the axis (perpendicular to the face) of the tube and

*Deceased

†Current Address : Institute of Chemical and Physical Research (RIKEN), Wako, Saitama, 351-0198, Japan

‡Current Address : Accelerator Laboratory, High Energy Accelerator Research Organization (KEK), Tsukuba, 305-0801, Japan

required installation of large amount of iron. Therefore, for this experiment we implemented a bucking coil system to more effectively cancel out the fringe fields.

2 Čerenkov detectors

2.1 Čerenkov detectors in HKS

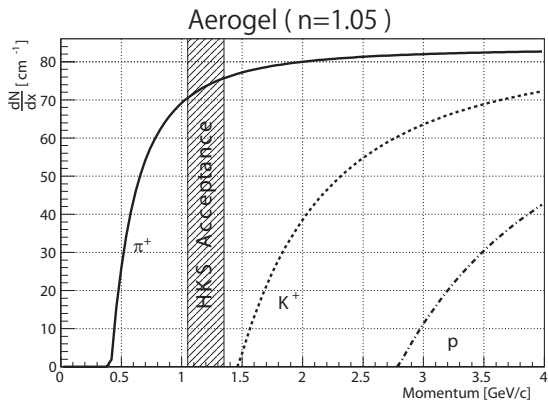


Figure 2: Number of Čerenkov photons per centimeter vs momentum in the aerogel medium ($n=1.05$). Only π^+ generate Čerenkov light within the HKS momentum acceptance. The aerogel Čerenkov detector is used as a veto detector to suppress π^+ particles.

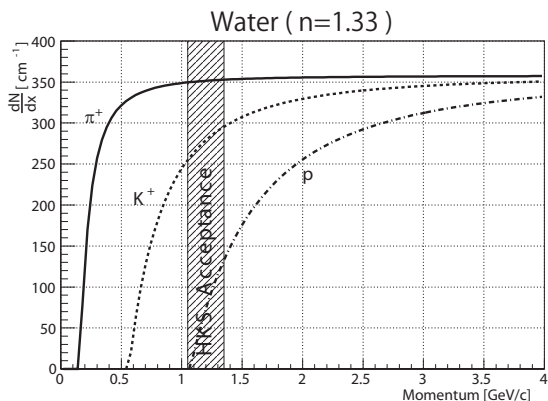


Figure 3: Number of Čerenkov photons per centimeter vs momentum in water ($n=1.33$). The water Čerenkov detector is used to separate p from other particles by choosing an optimized threshold of number of photoelectrons.

Over the HKS momentum acceptance of ~ 1.05 GeV/ c to ~ 1.35 GeV/ c , the number of background particles are 2,000:1 for protons and

10,000:1 for π^+ s relative to kaons. Using aerogel and water, Čerenkov detector index of refraction values of 1.05 and 1.33 were chosen. Figures 2 and 3 show predicted Čerenkov light photon yields for the three particle species in the two radiator media calculated by:

$$\frac{d^2N}{dx d\lambda} = \frac{2\pi\alpha z^2}{\lambda^2} \left(1 - \frac{1}{\beta^2 n^2(\lambda)}\right) \quad (1)$$

where N is the number of photons, α is the fine structure constant, λ is the wave length of the Čerenkov light, $n(\lambda)$ is the refraction index of the medium, and z and β are the charge and the velocity factor of the incident particle. In the figures, $n(\lambda)$ is fixed at 1.05 and 1.33 for aerogel and water, and the yield is integrated over a λ range between 300 nm and 600 nm, corresponding to the sensitive region of the PMTs. As the kaon and proton velocities are below threshold in aerogel, π^+ and lighter particles can be rejected. The water Čerenkov detector is sensitive to all three particle species, but can distinguish protons and kaons by the difference in photon yields.

2.2 Requirements

We required that a on-line rejection ratio of the order of 1/100 for π^+ and p to obtain the desired hypernuclear yield and signal to accidental background ratio. The goal of a high background rejection ratios must be balanced against the desire to maximize the efficiency of K^+ detection, particularly in the water Čerenkov detectors. This efficiency is determined by photo-electron collection efficiency of PMTs, a property that is strongly affected by magnetic fields.

A Monte Carlo simulation was done to estimate on-line background rejection ratios and kaon detection efficiency. This simulation was normalized with a cosmic ray tests which found, for the water Čerenkov detectors, a mean signal of 54 photoelectrons per cosmic ray. According to the simulation, two layers of water Čerenkov cuts that rejects 99.96% of protons will accept K^+ with a 94.5% efficiency. However, when the mean number of photoelectrons is reduced by 75% (mean signal of 13 photoelectrons), the K^+ acceptance rate drops to 75.7% for the same proton rejection ratio, directly reducing the yield for Λ hypernuclei. Given the limits on beam time, efforts to mitigate the effect of magnetic field on kaon detection efficiency are justified.

In order to maximize the yield of Λ hypernuclei and the signal to noise ratio, we set a goal that magnetic fields should not reduce photoelectron yields by more

than 35%.

3 Test of bucking coil

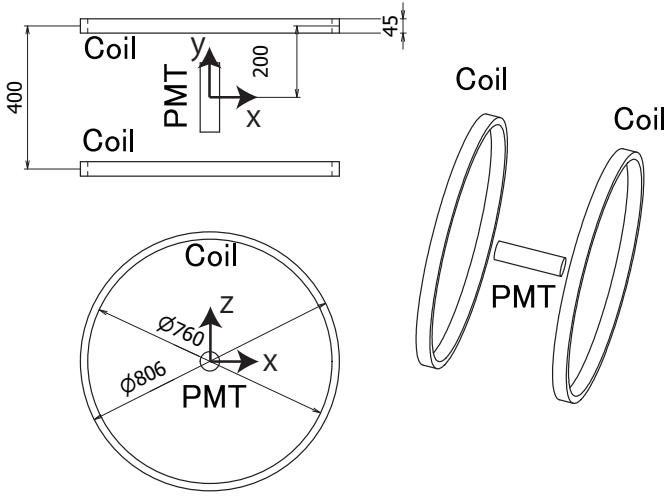


Figure 4: A schematic drawing of the setup of bucking coil test. An H7195 PMT was placed at the center of the two coils (Helmholtz coil). Unit in the figure is mm.

Before the setup of JLab experiment E05-115 was mounted, studies were made of the effects of magnetic fields on the Čerenkov PMTs and of the ability of bucking coils to cancel these effects. The test setup is shown in Fig. 4 which also defines the coordinate system. A two inches diameter H7195 PMT (HAMAMATSU, photocathode of bialkali, dynode stages of 12, supply voltage of -2000 V, typical gain of 3.0×10^6), which was used in the water Čerenkov detector, was tested.

3.1 Magnetic field generation

A Helmholtz coil which can generate magnetic fields to ~ 16 G was constructed. The cross section and the number of turns of each conductor are 45 mm \times 46 mm and 114, respectively. The excitation curve of the coil was measured by a hall probe (Group3 Technology, digital teslameter of DTM-151-DS, probe of MPT-141-10S, accuracy of $\pm 10^{-4}$) and compared to a calculation by OPERA3D-TOSCA[7] which is a magnetic field calculation software by using three dimensional finite element method in the Figure 5. The measured values of magnetic field of y-component (B_y) are lower by a few % than those of TOSCA

calculation. If the probe has small angles or/and little displacement from the center, the measured values could be lower than the real center value of B_y . In the present paper, the following values of magnetic field are derived from the applied current by using the measured relation.

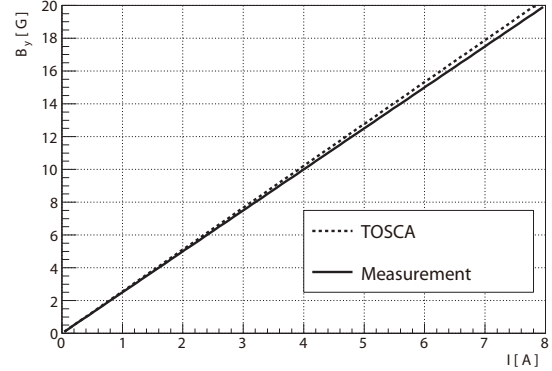


Figure 5: Magnetic field (B_y) and current (I) correlation at the center of the coils which are measured by the hall probe and calculated by OPERA3D-TOSCA[7].

The uniformity of the Helmholtz coil was also measured. In the range of 400 mm \times 400 mm around the center which we put PMT for the test, the uniformity of B_y was

$$\frac{B_y}{B_{y(\text{center})}} > 0.94 \quad (2)$$

The uniformity is checked by TOSCA as well. Figure 6 is showing $\frac{B_y}{B_{y(\text{center})}}$ by TOSCA calculation. The solid line describes the value when the values of x and y are fixed as 0 mm. The dashed line describes the value when the values of x and z are fixed as 0 mm. As seen in Figure 6, the TOSCA calculation shows $\frac{B_y}{B_{y(\text{center})}} > 0.94$ in the range of 400 mm \times 400 mm, which is consistent with the measurement within required accuracy for the bucking coil test.

The other components of magnetic field in the region of 400 mm \times 400 mm were

$$\frac{B_{x,z}}{B_{y(\text{center})}} < 0.03 \quad (3)$$

according to the measurements.

3.2 Light generation and circuit

An LED (STANLEY 3889S Yellow) was used as the light source for the gain study of PMT. The peak wave

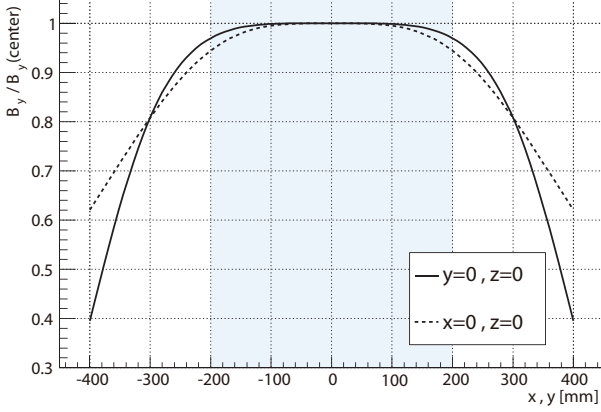


Figure 6: $B_y/B_y(\text{center})$ vs. displacement from the center of the coils by the TOSCA calculation. The solid line describes the value when the values of x and y are fixed as 0 mm. The dashed line describes the value when the values of x and z are fixed as 0 mm. The calculation is consistent with the measurement within required accuracy for the bucking coil test.

length and luminous intensity of the LED are 690 nm and 4 mCd. The LED was covered by a light diffusion cap in order to achieve uniform illumination of the PMT photocathode. The LED was placed at the bottom of a paper cylinder with an inside surface covered by a teflon reflector sheet. The distance between the bottom of the paper cylinder and the photocathode of PMT was 260 mm. The cylinder was wrapped with two turns of light-tight black sheets to prevent light leaks.

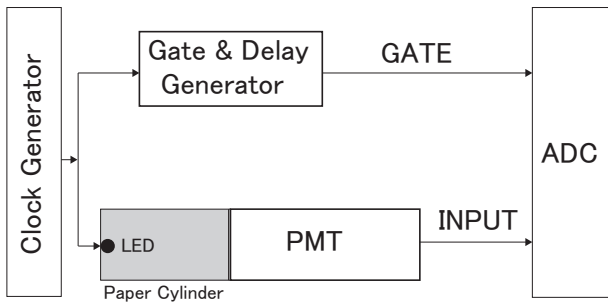


Figure 7: Electronics block diagram for the bucking coil PMT tests.

Figure 7 shows the electronics block diagram for the PMT tests. The LED generates light using Transistor-Transistor Logic (TTL) pulses from a

Clock Generator. The light intensity of the LED is controlled by varying the width of the pulses. The width was set at ~ 30 ns to generate ~ 200 photoelectrons. The charge information from the PMT was digitized by an Analog to Digital Converter (ADC) with a trigger derived from the LED drive signal.

3.3 Effect of magnetic field on PMT

Studies were made of the effects of magnetic fields on the PMTs before the bucking coils were installed. The results are presented as “relative gain”, which is defined as the ratio of ADC value with a magnetic field to the ADC value with no magnetic field. It should be noted that any change in “relative gain” would originate from multiple sources as 1) changes in the number of photoelectrons collected by the first dynode of the PMT and 2) changes in the amplification factor after the first dynode of the PMT.

3.3.1 Angular dependence

The θ is defined as the angle between the magnetic field direction (the y -axis) and the PMT axis (perpendicular to the face of the PMT) of the PMT. Figure 8 shows the angular dependence of the rela-

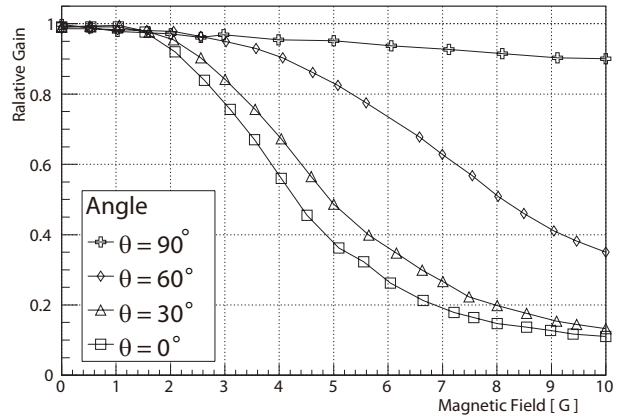


Figure 8: Relative gain of PMT as a function of magnetic field. PMT HV is set to -2000 V. Different markers represent different angles between the tube axis and magnetic field direction ($\theta = 0, 30, 60, 90$ degrees).

tive gain. The relative gain is more than 90% with $B_y < 2$ G for all θ . However, it drops to $\sim 40\%$ with a magnetic field of 5 G parallel to the PMT axis ($\theta = 0^\circ$). 5 G is the magnitude of the fringe field seen on these tubes in the spectrometer. As seen, the rela-

tive gain is strongly affected by magnetic fields along the axis of the PMT.

3.3.2 Effect on one photo-electron detection

The relative gain when using the LED is strongly affected by the magnetic field as discussed in the previous section. To see changes in the relative gain for a single photo-electron peak, data were taken with a self trigger. Figure 9 shows relative gain of one photo-electron peak as a function of magnetic field. The

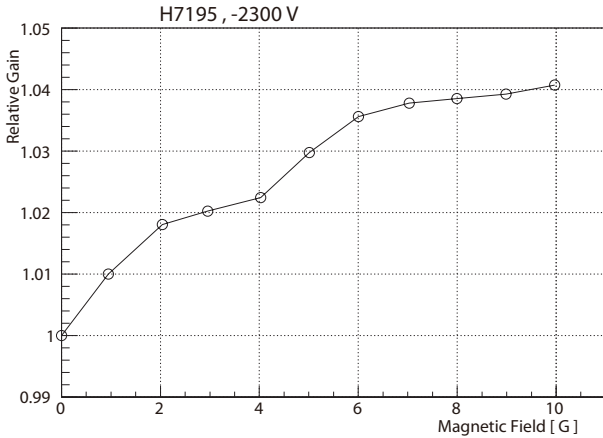


Figure 9: The relative gain of one photo-electron as a function of magnetic field. The applied HV on PMT (H7195) is -2300 V .

relative gain of one photo-electron is near to 1, and is slightly increasing with field. If the overall relative gain reduction originates only from that gain factor reduction after the first dynode, this result should show similar behavior to figure 8 when we used an LED trigger. In addition, a signal rate reduction was observed. According to these results, the reduction in relative gain originates mainly from a reduction of probability that electron which is converted from photon on photocathode reaches the first dynode of PMT.

It is also noted that the relative gain increase in figure 9 does not necessarily imply that gain factor is increased. Under higher magnetic fields, only higher energy electrons may be able to reach the first dynode. These higher energy electrons can knock off more secondary electrons at the first dynode, and what we observed might be biased by these events.

3.3.3 Applied HV dependence

Figure 10 shows the relative gain as a function of the magnetic field which is applied parallel to the axis of

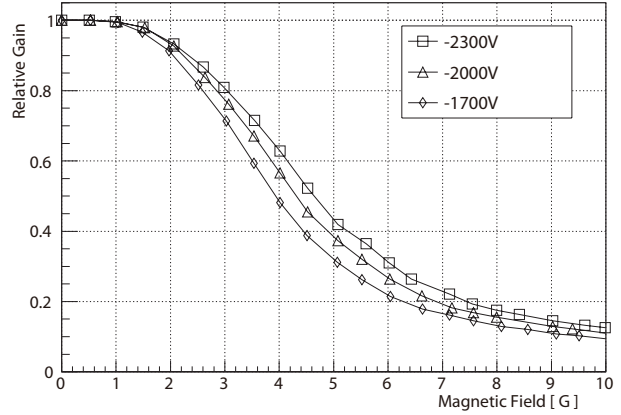


Figure 10: The relative gain as a function of the magnetic field with different HV settings of -2300 V , -2000 V and -1700 V for the PMT (H7195) .

the PMT ($\theta = 0^\circ$) with different HV settings. As the high voltage is increased, the effects of the magnetic field are eased slightly (e.g. the relative gain at 5 G are 0.42 for -2300 V and 0.31 for -1700 V). However, this improvement is insufficient for our experimental requirements.

3.4 Bucking coil test

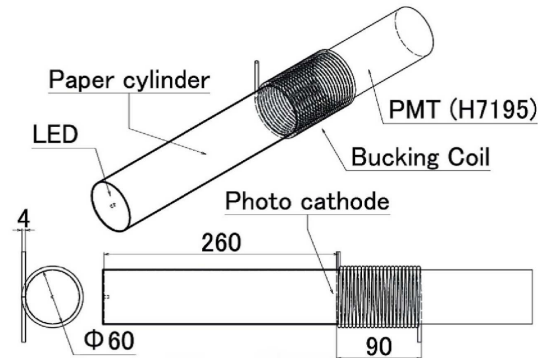


Figure 11: The setup of the bucking coil on PMT for the test. The bucking coil of 20 turns was wound around the PMT, starting at the photocathode and extending for 90 mm. Unit in the figure is mm.

Figure 11 shows setup of a bucking coil on a PMT as used for the tests. A wire with cross section of 4 mm^2 and a resistance of $0.2\ \Omega/\text{m}$ was used to wind the bucking coil. The wire of 20 turns was rolled onto the PMT, starting at photocathode making a coil with the length of 90 mm. The current applied to the bucking coil were set to cancel the magnetic field inside the

PMT.

The relative gain as a function of current for the bucking coil under magnetic fields of 4 G, 5 G and 6 G ($\theta = 0^\circ$) are shown in the Fig.12. The relative

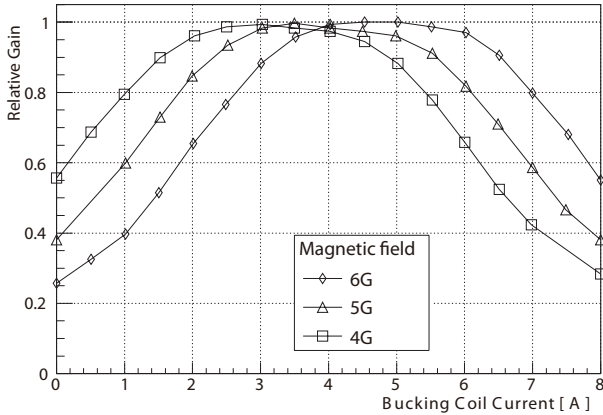


Figure 12: Relative gain as a function of the bucking coil current under magnetic fields of 4 G, 5 G and 6 G ($\theta = 0^\circ$). The length of bucking coil of 20 turns was 90 mm starting at the photocathode of PMT (H7195 , -2000 V).

gains were recovered to ~ 1 for each applied magnetic field on the PMT by choosing the optimal current for the bucking coil. Those curves have a plateau region. If one chooses bucking coil current of 2.5 A \sim 5.0 A, the relative gain is more than 0.95 under the magnetic field of 5 G.

3.4.1 Bucking coil position dependence

In the experiment, JLab E05-115, bucking coil cannot be rolled onto the PMT starting at the photocathode because of physical interferences from the frame of the Čerenkov detector. In anticipation of this constraint, tests were made with a bucking coil that started 40 mm away from the photocathode. The results are represented in the Fig.13. The relative gains are recovered to ~ 1 for each applied magnetic field as well as the Fig. 12. However, the necessary currents are higher than those of Fig. 12. This means that the relative gain is more sensitive to the magnetic field around the photocathode of the PMT.

3.4.2 Angular dependence

Figure 14 shows the relative gain as a function of the bucking coil current with angles of $\theta = 0, 30, 60$ and 90 degrees. As angles of the magnetic field with respect to the axis of PMT closer to 90° , the maximum

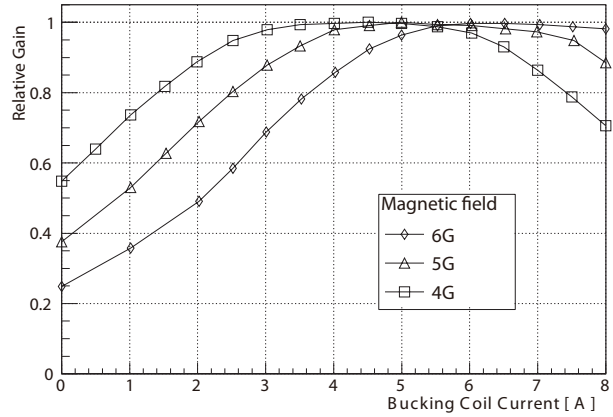


Figure 13: Relative gain as a function of the bucking coil current under magnetic fields of 4 G, 5 G and 6 G. The bucking coil started 40 mm away from the photocathode of the PMT (H7195 , -2000 V).

relative gains are lower though they are still more than 0.95 for $\theta = 90^\circ$. This imperfection of relative gain recovery is considered to be caused by a perpendicular component of magnetic field to the axis of PMT which cannot be cancelled by the bucking coil.

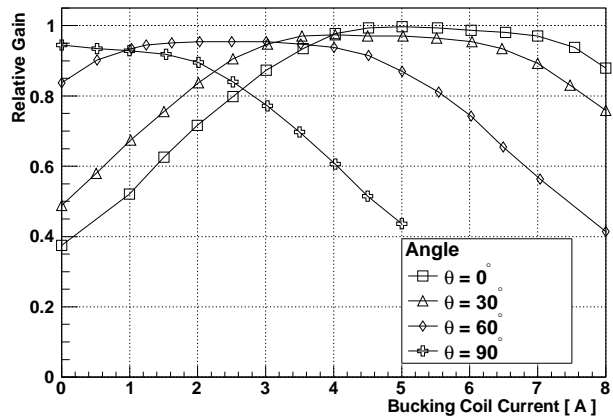


Figure 14: Relative gain as a function of the bucking coil current under a magnetic field of 5 G for the angles of $\theta = 0, 30, 60$ and 90 degrees (H7195 , -2000 V).

3.4.3 Number of turns dependence

A relation between relative gain and the number of bucking coil turns is shown in Fig. 15. In this test, a magnetic field of 5 G was applied on PMT ($\theta = 0^\circ$). The bucking coil started at the photocathode of the PMT, and a HV setting of -2000 V was used. Less

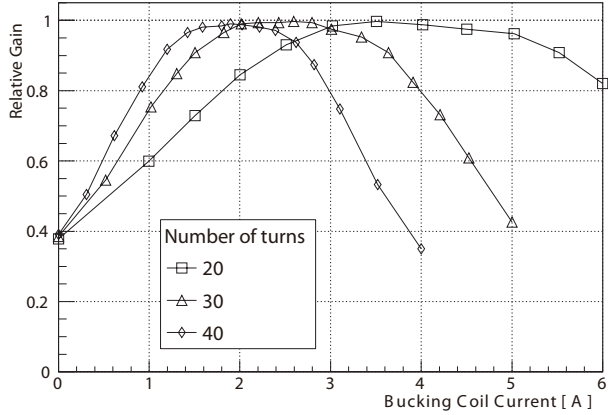


Figure 15: Relative gain as a function of bucking coil current with different number of bucking coil turns. A magnetic field of 5 G ($\theta = 0^\circ$) was used, and the bucking coil started at the photocathode of the PMT (H7195, -2000 V).

current is needed to recover the relative gain up to ~ 1 with coils with a greater number of turns though the plateau region becomes narrower.

3.4.4 HV dependence

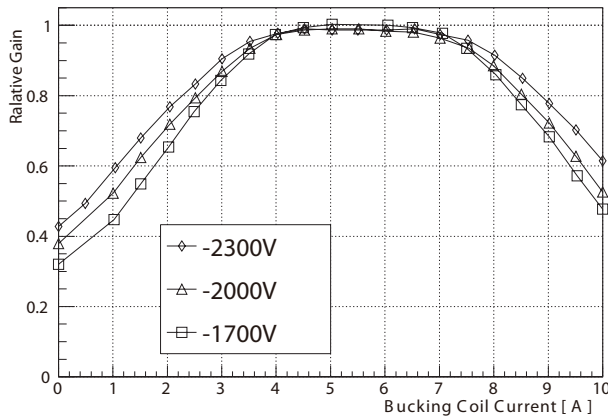


Figure 16: Relative gain as a function of the bucking coil current with different HV settings, -1700 V, -2000 V and -2300 V. A magnetic field of 5 G ($\theta = 0^\circ$) was applied, and the bucking coil position started at the photocathode of the PMT (H7195).

Figure 16 shows the relative gain as a function of bucking coil current with different HV settings, -1700 V, -2000 V and -2300 V. In this test, a magnetic field of 5 G was applied to the PMT ($\theta = 0^\circ$), and the bucking coil of 20 turns was wound start-

ing at the photocathode of the PMT. The necessary currents to recover relative gains up to ~ 1 for each HV setting are very similar. In the actual experiment setup, different HV settings were used for PMTs. The obtained results imply that a single bucking coil current can work though different HV settings are used in the actual experimental setup.

4 Bucking coil implementation for the experiment JLab E05-115

4.1 Water Čerenkov Detectors

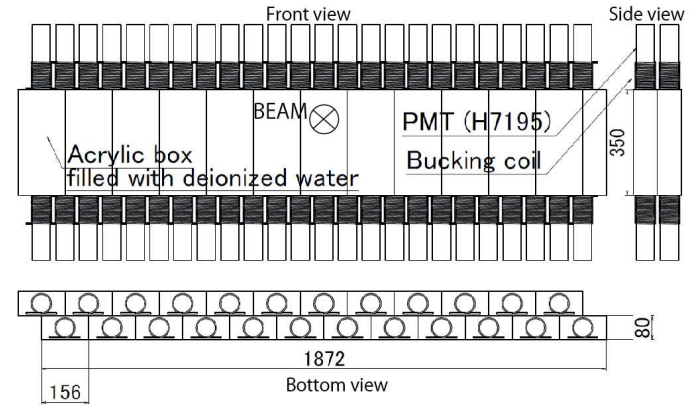


Figure 17: A schematic drawing of the water Čerenkov detector. There are two layers with 12 segments for each layer. A bucking coil of 40 turns was rolled around each PMT, starting ~ 40 mm away from the photocathode. Unit in the figure is mm.

A schematic drawing of the water Čerenkov detector is shown in the Fig. 17. There are two layers of water Čerenkov detector with 12 segments for each layer. A detector segment consists of an acrylic box with its inside surface covered by a teflon sheet, and PMTs (H7195) on top and bottom of the box with UV-glass windows. Deionized water (resistivity of 18 M Ω -cm, the refraction index of 1.33) was used as the radiation medium. A bucking coil of 40 turns was rolled around each PMT, starting ~ 40 mm away from the photocathode. Figure 18 is a photograph of bucking coils on PMTs of the water Čerenkov detectors.

In the experiment, the effects of bucking coil for the water Čerenkov detector were checked by measuring the counting rates of each PMT, which is equivalent to measuring the relative gains as discussed in section 3.3.2 if the discriminator threshold is kept the same.



Figure 18: A photograph of the bucking coils on the PMTs of water Čerenkov detectors. A bucking coil of 40 turns was used for each PMT.

The ratios of counting rates of each PMT when the HKS dipole magnet was on to those when the magnet was off are shown in the Fig. 19. The counting rates for each PMT are decreased by more than $\sim 50\%$ when the bucking coil is not used. On the other hand, the counting rates with bucking coil ON (40 turns, the current of 2 A) are recovered to those with no HKS magnetic field.

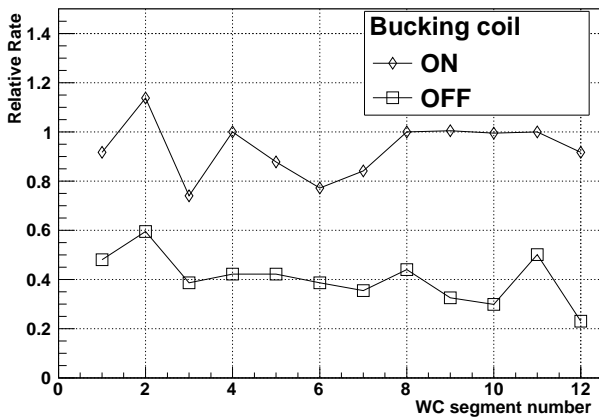


Figure 19: Relative rates of each segment of the first layer of water Čerenkov detectors when the HKS dipole magnet is on. The relative rates are recovered up to ~ 1 when the bucking coils are ON (40 turns , the current of 2 A).

4.2 Aerogel Čerenkov detectors

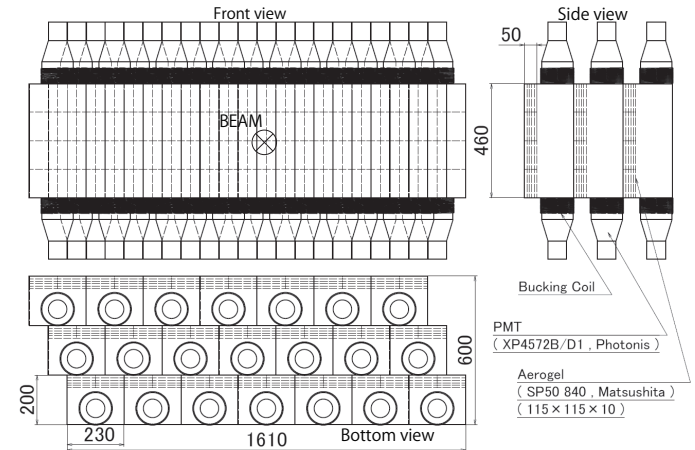


Figure 20: A schematic drawing of the aerogel Čerenkov detector. There are three layers with 7 segments for each layer. Unit in the figure is mm.

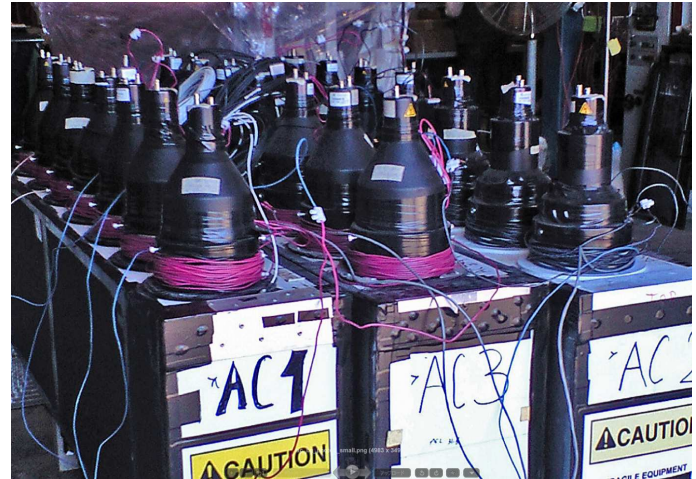


Figure 21: A photograph of the aerogel Čerenkov detectors. Bucking coils are rolled around the photocathodes of each PMT.

Figure 20 shows a schematic drawing of the aerogel Čerenkov detector. There are three layers of aerogel Čerenkov detectors, and each layer has 7 segments. A segment consists of a structurally strengthened paper box, 40 pieces of hydrophobic silica aerogel tiles (SP-50 , Matsushita¹ , refraction index of 1.05) and two PMTs (XP4572B/D1, Photonis, photocathode of bialkali, dynode stages of 10, typical supply voltage of +2100 V, typical gain of 2.0×10^7), located on the top and bottom of the box without any windows.

¹Currently produced by the Japan Fine Ceramics Center

It is noted that the PMT which is used for aerogel detector is more sensitive to magnetic fields because its diameter (5 inches) is larger than that for water Čerenkov detector (2 inches).

Figure 21 shows the bucking coils on PMTs for the aerogel Čerenkov detectors. 40 turns of bucking coils were used for each PMT. Figure 22 shows the relative gain of the each PMT in the first layer of the aerogel Čerenkov detectors as a function of bucking coil current. Because the fringe field of the HKS dipole is not uniform in the region of the aerogel Čerenkov detector, the optimal bucking coil currents are different for each segment. However, a single current of 8 A was chosen since it recovered most of the relative gain reasonably for all PMTs.

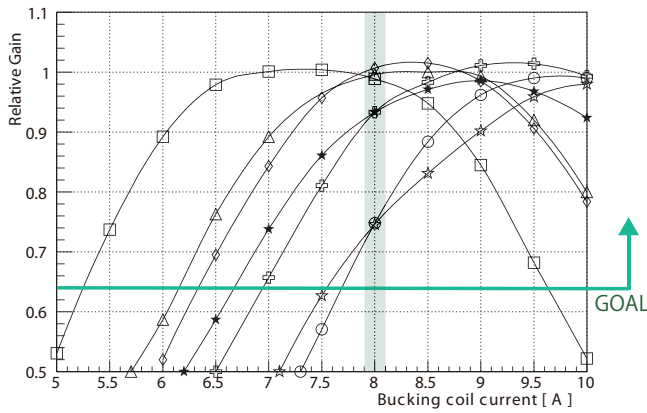


Figure 22: Relative gain of each segment of the first layer of aerogel Čerenkov detectors. In the experiment, a single current of 8 A was chosen for all PMTs.

4.3 K^+ identification performance

A schematic drawing of the HKS detectors is represented in the Fig. 1. The HKS consists of three layers of plastic scintillation detectors (KTOF1X , KTOF1Y , KTOF2X) for TOF (Time Of Flight) measurement, two layers of horizontal drift chambers (KDC1 , KDC2) for particle tracking, and the aerogel and water Čerenkov detectors (AC1 , AC2 , AC3 , WC1 , WC2) for particle identification.

4.3.1 On-line K^+ identification

The HKS trigger was made by the following logical condition,

$$\text{HKS}_{\text{trigger}} = \text{CP}_{\text{trigger}} \otimes K_{\text{trigger}} \quad (4)$$

where,

$$\text{CP}_{\text{trigger}} = \text{KTOF1X} \otimes \text{KTOF1Y} \otimes \text{KTOF2X}, \quad (5)$$

$$K_{\text{trigger}} = \overline{\text{AC}} \otimes \text{WC}. \quad (6)$$

$\text{CP}_{\text{trigger}}$ in eq.(5) is a charged particle trigger which consists of the coincidence of three layers of TOF detectors (KTOF1X , KTOF1Y and KTOF2X). In eq. (6), AC represents $(\text{AC1} \otimes \text{AC2}) \oplus (\text{AC2} \otimes \text{AC3}) \oplus (\text{AC3} \otimes \text{AC1})$, and WC represent $(\text{WC1} \otimes \text{WC2})$. The overline on AC means that the AC was used as veto to suppress π^+ . The typical HKS trigger rate was ~ 1 kHz with a beam current of $2 \mu\text{A}$ on a polyethylene target (CH_2 , the material thickness of $450 \text{ mg}/\text{cm}^2$).

Data with the $\text{HKS}_{\text{trigger}}$ and the $\text{CP}_{\text{trigger}}$ conditions were taken during the experiment although a coincidence between the HKS trigger ($\text{HKS}_{\text{trigger}}$) and the HES trigger was used for physics data. π^+ and p rejection ratios were estimated by comparing the number of those events in the $\text{HKS}_{\text{trigger}}$ and the $\text{CP}_{\text{trigger}}$. The rejection ratios of π^+ and p with a beam current of $2 \mu\text{A}$ on the polyethylene target were 7.4×10^{-3} and 3.8×10^{-2} , respectively. The K^+ detection efficiency was 91%.

4.3.2 Off-line K^+ identification

At the on-line (hardware) trigger level, thresholds of the Čerenkov detectors were set slightly loose so as to avoid over-cutting of K^+ s. Therefore, some π^+ s and protons remained in the recorded data. The top plot of Fig. 23 shows the correlation between number of photoelectrons from the sum of the three layers of aerogel Čerenkov detectors and mass squared of the measured particle. The bottom plot is an x-projection of the top graph. Mass squared, m^2 is calculated by the following equation,

$$m^2 = \frac{k^2}{(1/\beta^2) - 1} \quad (7)$$

where k is the momentum reconstructed by transfer matrix of the HKS, and β is the velocity factor derived from the TOF measurement. In Fig. 23, clusters of π^+ , K^+ and p are clearly seen. π^+ s are rejected by applying the cut on the number of photoelectrons in the aerogel Čerenkov detector.

Two types of boxes of water Čerenkov detectors were used in the experiment. The main differences between them were reflective materials and PMT choice.

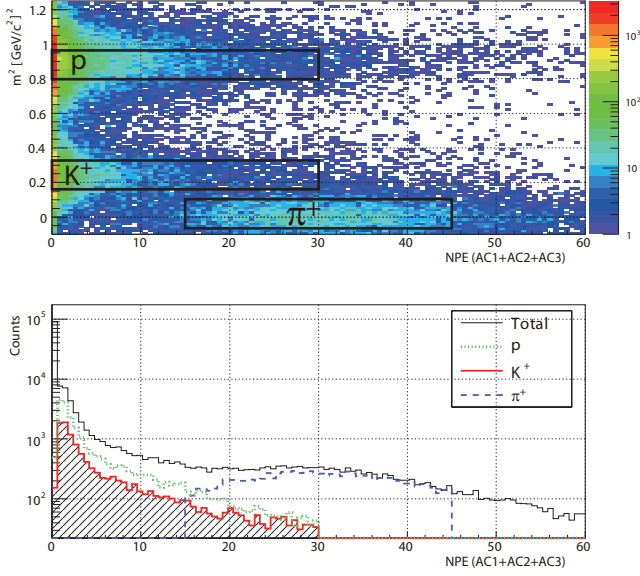


Figure 23: Correlation between the number of photoelectrons summed over the three layers of the aerogel Čerenkov detector and mass squared (top), and the x-projection of the top figure (bottom).

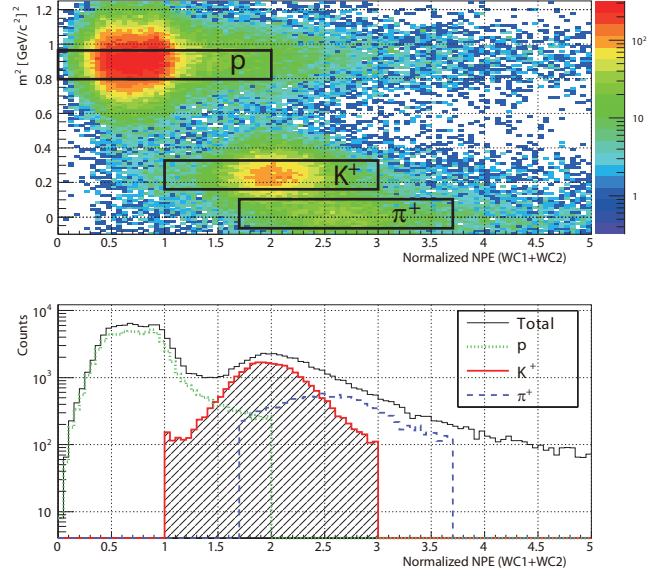


Figure 24: Correlation between normalized number of photoelectrons from the sum of two layers of water Čerenkov detectors and mass squared (top), and the x-projection of the top figure (bottom).

On the low momentum side (segment numbers from 1 to 6, BOX1), white acrylic as reflective material and H7195 PMTs were used. On the high momentum side where severer particle identification is required (segment numbers from 7 to 12 , BOX2), teflon sheets as the reflective material and H7195UV PMTs which has UV-glass window were used. H7195UV has the same responses to the magnetic field as H7195, but higher efficiency to ultra violet light.

In cosmic ray tests, the average number of photoelectrons in BOX1 and BOX2 type segments were ~ 50 and ~ 100 , respectively. There was difference of number of photoelectrons between BOX1 and BOX2, and thus, normalized number of photoelectrons were introduced to adjust K^+ peak to 1. The top plot of Fig. 24 shows the correlation between the normalized number of photoelectrons from the sum of two layers of water Čerenkov detectors and the mass squared, while the bottom plot is the x-projection of the top figure. Protons and other particles (π^+ , K^+) can be separated by the cut on the number of photoelectrons.

Figure 25 shows the mass squared distribution before and after the cuts on the number of photoelectrons in the Čerenkov detectors. K^+ events are clearly selected after applying these cuts. When the Čerenkov and mass squared cuts were selected to keep 90% kaons in the total off-line events, the contaminated π^+ and p events were 4% and 3% of remaining

events (using the 450 mg/cm² CH₂ target). In this case, the total (on-line and off-line) rejection powers of π^+ and p were 6.5×10^{-4} and 6.1×10^{-5} , respectively.

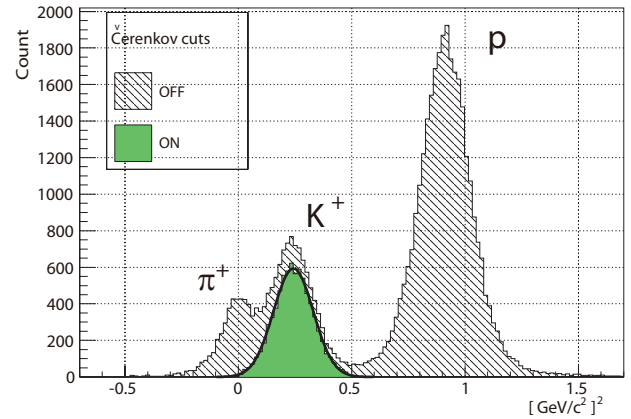


Figure 25: Mass squared distribution before and after the cuts on the Čerenkov detectors. K^+ events are clearly selected after the cuts. The width of single gaussian fitting for kaon peak is $\sigma \sim (0.29 [GeV/c^2])^2$.

5 Summary

The water and aerogel Čerenkov detectors, which were located a few meters away from the HKS dipole magnet, needed to be operated in a fringe field of ~ 5 G. The separation efficiency of K^+ from the other background particles (π^+ and p) is deteriorated in these fields as the fields reduce the relative gains. Monte Carlo simulations indicated that relative PMT gains of more than 65% were required to keep the yield of Λ hypernuclei and the signal to noise ratio reasonably high. To operate the PMTs attached to Čerenkov radiators under this field, bucking coils were installed to actively and locally cancel the magnetic field on the PMTs.

Tests with a Helmholtz coil were performed to study the effects of magnetic fields on the H7195 PMT which was used for the water Čerenkov detectors. With a magnetic field of ~ 5 G parallel to the axis of the PMT, the gain was reduced by 60% (relative gain of 0.40). A bucking coil of 40 turns and ~ 2 A starting at the photocathode of PMT was needed to recover the relative gain up to ~ 1 in this case.

In JLab E05-115 experiment, bucking coils of 40 turns and current of 2 A were used for the water Čerenkov detectors, and coils with 40 turns and current of 8 A were used for aerogel Čerenkov detectors. With these coils, a relative gain of more than 0.70 and 0.75 for each segment of the water and aerogel Čerenkov detectors, respectively, were achieved. The on-line rejection ratios of π^+ and p with a beam current of $2 \mu\text{A}$ on the CH_2 target (the material thickness of 450 mg/cm^2) were 7.4×10^{-3} and 3.8×10^{-2} , respectively. The efficiency for K^+ events was 91%. Off-line, K^+ events were selected by applying cuts on the number of photoelectrons in the Čerenkov detectors. When Čerenkov and mass squared cuts were selected to keep 90% efficiency in off-line kaon selection, the contaminated π^+ and p events were 4% and 3% of remaining events (using the 450 mg/cm^2 CH_2 target). In this case, the total (on-line and off-line) rejection powers of π^+ and p are 6.5×10^{-4} and 6.1×10^{-5} , respectively. The implementation of bucking coils allowed for a very clean on-line and off-line selection of K^+ events.

Acknowledgements

We would like to thank JLab staff of physics, accelerator and engineer divisions for supports for the experiments. The program at JLab's Hall-C is supported

by the Specially promoted program (12002001), the Creative research program (16GS0201), Grant-in-Aid by MEXT (15684005), Japan, JSPS Research Fellowships for Young Scientists (244123), US-Japan collaboration research program, the JSPS Core-to-Core Program (21002) and the Strategic Young Researcher Overseas Visits Program for Accelerating Brain Circulation (R2201) by the Japan Society for Promotion of Science. This work is supported by U.S. Department of Energy contract DE-AC05-06OR23177 under which Jefferson Science Associates, LLC, operates the Thomas Jefferson National Accelerator Facility.

References

- [1] O.Hashimoto, S.N.Nakamura, L.Tang, J.Reinhold et al., JLab E05-115 proposal (2005)
- [2] O.Hashimoto et al., Nuclear Physics A835 , 121-128 (2010)
- [3] L.Yuan et al., Physical Review C73 , 044607 (2006)
- [4] L.Tang et al., Nuclear Physics A790 , 679c-682c (2007)
- [5] O.Hashimoto et al., Nuclear Physics A804 , 125-138 (2008)
- [6] S.N.Nakamura et al., Physical Review Letters 100 , 012502 (2013)
- [7] <http://www.cobham.com> , Cobham Antenna Systems, Vector Fields Simulation Software